Chapter 2

Experimental Methods

The experiments documented in this thesis were carried out at the Nuclear Physics Department of the Australian National University (ANU) and at the Legnaro Laboratories of the National Italian Nuclear Physics Institute (INFN) in Padua, Italy. This chapter gives an account of the experimental methods which have been used.

2.1 Beam Production and Acceleration

In all experiments a beam of projectile ions was accelerated and directed onto a target foil in which the nuclear reactions took place. The projectile ions were produced in an ion-source at the beginning of the accelerator in the 1^- charge state, i.e. with one excess electron. The initially negative charge state enables a tandem acceleration using the same positive electrostatic potential. After the first acceleration boost due to attraction, the ions pass through a thin carbon foil and some electrons are stripped off resulting in a positive charge state. Subsequently, the ions receive a second boost of acceleration by repulsion.

2.1.1 Negative Ion Sources

At the Nuclear Physics Department of the ANU a *Cesium Beam Sputter Source* and an *Inverted Sputter Source (SNICS)* are in operation to produce negative ion beams[1,2]. At the Legnaro Laboratories similar ion sources exist.

The Cesium Beam Sputter Source is based on a design by Middleton and Adams[3,4]. In this source the projectile ions are sputtered from a hollow conical target on the source axis by a 20 - 30 keV, 1 - 2 mA beam of Cs^+-ions. The Cs^+-ions are generated by evaporation of Cs-atoms from a reservoir of liquid cesium through a tungsten ionizer. The cesium atoms are absorbed in the porous tungsten which is heated to a temperature of typically 1100 - 1200°C, so that the atoms diffuse through the metal and evaporate on the surface. The work function of the tungsten surface is of the order of the ionization potential of cesium. Therefore a large proportion of the evaporating cesium is emitted as positive Cs^+-ions. The Cs^+-ions which emerge from the ionizer surface are extracted by an accelerating-decelerating electrode system and bombard the target cone. The low ionization potential of

[1]R. Middleton, *Treatise on Heavy-Ion Science* 7, ed. D.A. Bromley, NY (1985) 53.

[2]R. Middleton, Nuc. Inst. Meth. **122** (1974) 35.

[3]R. Middleton, C.T. Adams, Nucl. Inst. Meth. **118** (1974) 329.

[4]K.N. Leung, *The Physics and Technology of Ion Sources*, ed. I.G. Brown, Wiley, NY (1989).

cesium, 3.87 V, causes a relatively large proportion of negatively charged ions to be sputtered from the cone. Usually a number of cones is mounted on a revolving wheel, so that ion species can be changed quickly.

The source can be run in direct or reverse mode. In direct mode the Cs^+-beam sputters directly from the cone and the negative ions are extracted through holes in the cone. In reverse mode the Cs^+-ions pass through the hole in the cone which is on a negative potential of approximately -20 keV. After passage they are reversed by the extraction electrode which is on ground potential. The Cs^+-beam then sputters ions from the rear side of the cone and the extraction process of the negative ions is not hindered by the cone as in the direct mode, so that larger beam currents of negative ions can be obtained. In both cases the intensity of the Cs^+-beam and the resulting negative ion beam are controlled by the temperature of the ionizer and the cesium reservoir. Negative ions from gaseous elements can be produced by introducing the gas through an inlet pipe into the target cone region. In the SNICS an annular ionizer is used and the negative ions are extracted through the hole in the ionizer. The advantage of this source is the simple geometry which allows higher beam intensities to be extracted.

Typical ion beams extracted from these sources can be of the order of tens of μA, but depend strongly on the electron affinity of the element. For elements with small or zero electron affinity, as e.g. the noble gases, ion beams cannot be generated. In some cases, as e.g. nitrogen and the alkali metals, negative ions can only be produced in form of their hydrogen compounds.

2.1.2 Beam Acceleration

The Nuclear Physics Department of the ANU operates a tandem Van de Graaff accelerator[5–7] to produce beams of heavy ions up to energies of the order of 50 – 150 MeV. A similar machine exists in Legnaro, so that the description in this section applies accordingly. The beam of negative ions produced by the ion source is analysed by a 90° magnet, in which the desired ions in the charge state 1^- are separated from other, contaminant isotopes and charges states. The analysed beam is then injected into the Van de Graaff tandem. In the accelerator the negative ions are initially boosted from ground potential towards the positively charged high

[5] *Large Electrostatic Accelerators*, Nucl. Inst. Meth. **122** (1974) 1.

[6] J.B.A. England, *Techniques in Nuclear Structure Physics*, Macmillan Press, London (1974).

[7] T.R. Ophel *et al.*, Nucl. Inst. Meth. **122** (1974) 227.

voltage terminal in the centre of the machine to obtain an energy of

$$E = eU \tag{2.1}$$

where e is the charge constant and U the terminal voltage. Terminal voltages of up to $U = 16$ MV are used in standard operation. In the ANU machine the terminal is charged by a system of three revolving Pelletron chains[8-11]. The pellets are charged at ground and de-charged at the high-voltage terminal by induction electrodes. The induction voltages between electrode and pellet are typically 50 keV. At a chain speed of 15 m/s the charging current of the system is approximately 150 μA using both upward and downward charge transport.

The terminal and the charging system are contained and insulated in a high pressure vessel filled with SF_6 gas at $5 \cdot 10^5$ Pa to ensure stable high voltage conditions. The beam travels from source to target through an evacuated beam tube which has inside the machine an aperture of 45 mm. The operational pressure in this tube is maintained by titanium getter pumps and is typically $2 \cdot 10^{-5}$ Pa except at the ion source where escaping source plasma leads to an increase in pressure by a factor of about 100.

Inside the terminal the negative ions penetrate through a carbon foil or a gas target where electrons are stripped off due to collisions with carbon or gas atoms[12,13]. This results in a distribution of positive charge states[14,15]. The most intense charge state q^{max} can be evaluated from the semi-empirical formula

$$q^{max} = Z(1 + [Z^{-0.45} \cdot 3.85 \cdot \sqrt{E/A}]^{-1.67})^{-0.6} \tag{2.2}$$

where E (in MeV) is the energy obtained by the ions in the initial acceleration phase. For an injected $^{16}O^-$ beam and the maximal terminal voltage of 16 MV this gives $q^{max} \simeq 6.3$, indicating that 6^+ is the most intense charge state for this beam.

The positively charged ions experience a second phase of acceleration back to the ground potential at the other end of the machine. The final energy after the second

[8] R.J. Van de Graaff, K.T. Compton, L.C. Van Atta, Phys. Rev. **43** (1933) 158.

[9] L.C. Van Atta, R.J. Van de Graaff, H.A. Barton, Phys. Rev. **43** (1933) 149.

[10] R.G. Herb, Inst. Elec. Electron. Engrs., Trans. Nucl. Sci. NF **18**, 3 (1971) 71.

[11] R.G. Herb, Nucl. Inst. Meth. **122** (1974) 267.

[12] H.D. Betz, Rev. Mod. Phys. **44** (1972) 465.

[13] J.L. Yntema, Nucl. Inst. Meth. **122** (1974) 45.

[14] S.A. Savoy, M.Sc.-Thesis, Kansas State University, *unpublished* (1972).

[15] A.B. Wittkower, H.D. Betz, Atomic Data **5** (1973) 113.

acceleration phase for oxygen ions in the $q^{max} = 6^+$ charge state and $U = 16$ MeV is then

$$E_{lab} = (1 + 6) \cdot eU = 112 \text{ MeV} \tag{2.3}$$

After the beam leaves the tandem accelerator a specific charge state, often q^{max}, is selected from the charge state distribution using a 90° analysing magnet. Higher charges states may be selected to give higher energies. The selected beam is then transported to the experimental set-up.

The terminal voltage of the accelerator is stabilized using a feed-back system. The beam is focused by the 90° analysing magnet to a point after the bend. At this focal point there is a collimator. If the beam moves to one side of the collimator then the current induced by the beam on this side of the collimator will increase with respect to the other side where it decreases. Any change of the beam on the collimator is due to changes in the beam energy. The differential signal from the collimator is therefore used to correct the terminal voltage and thus the beam energy. This is achieved by altering the corona discharge current drawn from the high voltage terminal. A beam energy variation of less than 10 keV can be achieved.

The beam energies are defined by the magnetic field in the 90° analysing magnet. The field strength is measured with a nuclear magnetic resonance probe. For the ANU machine several calibration measurements[16] have demonstrated that the energy definition achieved in this way is better than 0.04%. Thus for bombarding energies of the order of 100 MeV the beam energy is defined to ±40 keV.

In the measurements of the excitation functions discussed in this work the magnetic field was changed in only one direction to avoid differential hysteresis effects in the 90° analysing magnet. This ensures optimum energy definition. If certain energies had to be repeated or if a monotonic increase or decrease of the field strength was not possible for other reasons, the magnet was run from zero to full strength to zero in several cycles before setting it to the intended value. This procedure has been found to guarantee that the consistency of the monotonic sweep is retained.

After acceleration the beam of projectile ions is focused on a target in which the nuclear reactions take place. The targets used in this work were typically in the form of a strip, 1 mm wide and 50 μg/cm^2 in thickness, evaporated or sputtered[17] onto a carbon backing of 20 μg/cm^2. The target materials were close to 100% enriched in the isotope to be investigated.

[16]R.H. Spear *et al.*, Nucl. Inst. Meth. **147** (1977) 455.

[17]H.L. Adair, E.H. Kobisk, *Treatise on Heavy-Ion Science* 7, ed. D.A. Bromley, NY (1985) 53.

2.2 Energy and Time Measurements

The work presented in this thesis is concerned with excitation functions for fusion and scattering of the nuclear binary system. In order to establish the fusion and scattering cross sections for a particular bombarding energy, the products of the nuclear reactions in the target foil have to be identified. This can be achieved through measurements of their *energy loss* in a medium, their energy deposition when stopped, which is referred to as *residual energy*, and their *time-of-flight* over a certain distance[18,19]. The combination of the information from two of these measurements in many cases allows the identification of the reaction products.

2.2.1 Energy Loss Measurements

When an ion in a certain charge state, e.g. a reaction product, passes through a gas detector, it ionizes the gas molecules. If the gas detector operates as an ionization chamber or in the proportional regime, the integrated charge is proportional to the energy loss, which itself depends on the charge state, the mass and the energy of the ion[20]. This can be approximately expressed as

$$-\frac{dE}{dx} \propto \frac{mZ_{eff}^2}{E} \tag{2.4}$$

where dE is the energy loss over the differential distance dx and Z_{eff} is the effective charge state of the ion. For light ions it is $Z_{eff} = Z$.

Equation 2.4 suggests the use of a detector system consisting of a gas-detector, which measures the energy loss ΔE over a small distance Δx with

$$\Delta E \equiv \frac{dE}{dx}\Delta x, \tag{2.5}$$

followed by a measurement of the residual energy E_{res}. The sum of ΔE and E_{res} gives the particle's energy E. In a plot of ΔE versus E for a fixed mass m different charge states correspond to segments of hyperbolae which have their vertices at different points of the diagonal $\Delta E = E$. Often the energy loss ΔE is small compared to the residual energy E_{res}, so that the latter can in good approximation be identified with the particle energy E. This method has been employed in this

[18] G.F. Knoll, *Radiation Detection and Measurement*, Wiley, N.Y. (1989).

[19] W.R. Leo, *Techniques for Nuclear and Particle ...*, Springer, Berlin (1987).

[20] F.S. Golding, *Treatise on Heavy-Ion Science* 7, ed. D.A. Bromley, New York (1985) 227.

work to identify quasi-elastic scattering at backward angles. It enabled the isolation of contributions with different atomic numbers Z to the quasi-elastic scattering cross section.

A second particle identification technique uses instead of the kinetic energy the time-of-flight (TOF) of the reaction products. The kinetic energy E of a reaction product is given by

$$E = \frac{mv^2}{2} \tag{2.6}$$

which can be combined with Equation 2.4 to yield

$$-\frac{dE}{dx} \propto \frac{Z_{eff}^2}{v^2} = \frac{Z_{eff}^2 t^2}{d^2} \tag{2.7}$$

where t is the time-of-flight over the fixed distance d. Thus, in a two-dimensional spectrum of TOF versus energy loss ΔE, ions with comparable velocities can be separated according to their effective charge states. This method has been used in this work to identify the fission fragments resulting from fusion-fission of ^{32}S + ^{208}Pb.

The energy loss ΔE in a medium is most easily measured with a gas detector operating as ionization chamber. This was the set-up in the quasi-elastic backscattering experiments. The reaction product passing through the gas volume generates positive ions and negative electrons by ionizing the gas molecules. Due to the thermal motion which results in collisions between the charge carriers, the charges would eventually recombine. It is therefore necessary to apply an external electrical field to collect the charge carriers before they can recombine. As a consequence of the smaller energy loss of the light electrons in collisions with gas molecules, as compared to the heavy positive ions, the electrons can be collected much faster. The collection times for the two charge carriers differ typically by a factor of about 100. However, even small contaminations of the gas by strongly electronegative molecules like H_2, O_2 or halogens lead to the formation of negative ions which reduce the collection time for negative charge carriers dramatically. Thus particularly suitable gases for ionization detectors are clean electropositive gases like noble gases or carbon-hydrogen compounds. In this work propane was used.

When the electric field strength is large, the charge carriers gain enough kinetic energy before collection to ionize neutral gas molecules. This leads to an amplification of the signal. With a properly chosen field strength amplifications by a factor of 10^4 can be achieved. Under these conditions the final ionization current is proportional to the energy loss ΔE, so that the performance of the detector is

referred to as the *proportional regime*. The multi-wire proportional counters of the fission fragment spectrometer operate in this regime. The magnitude of the field strength necessary to operate a gas detector in the proportional regime depends on the gas filling and the gas pressure. Typical field strengths are $\mathcal{E} \gtrsim 1$ kV/cm.

If the gas volume is large, the energy and timing resolution of the detector is reduced, because of varying distances between particle track and anode. The use of a Frisch-grid close to the anode can compensate for this effect, when the bias voltages are chosen, so that the larger part of the potential difference occurs between the anode and the Frisch-grid. Thus independent from the location of the particle track, the main amplification of the electron-signal occurs between the grid and the anode. The performance of a gas detector can further be improved, when the gas volume is not static, but when it is constantly replaced. This can be achieved with a gas-flow system. In this case contaminants which may accumulate over time are removed.

2.2.2 Measurement of the Residual Energy

The residual energy E_{res} of reaction products has been measured in this work with silicon surface barrier detectors[21,22]. Any energy deposited in a silicon surface barrier detector, which is based on a semiconductor junction, causes the creation of electron-hole pairs. The average energy needed for this process at room temperature is $\epsilon = 3.62$ eV. This compares with typically 15–30 eV for the creation of a pair of charge carriers in a gas detector and indicates that the energy resolution of semi-conductor detectors is generally much better than that of gas detectors. Not all of the 3.62 eV is needed to lift the electron into the conduction band, since the band gap is only 1.115 eV. Some of the energy is released to the lattice in form of phonons.

If all of the energy deposited by the reaction product in the detector would be used to overcome the band gap, no fluctuations would occur in the number of electron-pairs produced by reaction products of given energy. On the other hand, if the energy partition between phonons and electrons would be statistical, the number of electron-hole pairs n would obey Poisson statistics and there would be a variance of $\langle n \rangle = \sqrt{n}$. In fact, initially a shower of very energetic electrons is created. The energy is then spread over several generation of electrons until the energy of each

[21]G.F. Knoll, *Radiation Detection and Measurement*, Wiley, NY (1989).

[22]EG&G ORTEC *Modular Pulse-Processing Electronics...* (1995).

electron is reduced to a few eV and electron-hole pairs are created. Since this is a complicated process, it has only been possible to describe it phenomenologically using the Fano factor F. The variance of n is then

$$F\langle n\rangle = F\sqrt{n} \tag{2.8}$$

so that the energy resolution in terms of the full-width-at-half-maximum ($FWHM$) is given by

$$\Delta E_{FWHM} = 2.35\sqrt{FE\epsilon} \tag{2.9}$$

where E is the energy of the reaction product. The value of the Fano factor for silicon is $F \approx 0.12$. Thus the intrinsic energy resolution of a silicon surface barrier detector for the detection of a 35 MeV reaction product is of the order of 10 keV.

However, in practice the energy resolution is reduced by electronic noise due to the leakage current, the capacitance and due to the bias resistor of the detector. In addition, energy loss and straggling in the detector entrance window result in a broadening of the energy definition. These effects are increased, if particles enter the detector at different angles. When the detector is used at the end of a detection telescope, the energy resolution is further worsened by the energy deposition in the preceding detectors. For α-particles detected by a silicon surface barrier detector an energy resolution of better than $\Delta E_{FWHM} \simeq 20$ keV can be achieved. The energy of elastically scattered ^{16}O nuclei at $E_{lab} = 73\ MeV$ at backward angles could be resolved in this work with a resolution of $\Delta E_{FWHM} \simeq 300$ keV by using a silicon surface barrier detector which was preceded by a gas detector.

2.2.3 Measurement of the Time-of-Flight

From Equation 2.6 it follows that

$$E = \frac{m}{2}\frac{d^2}{t^2} \tag{2.10}$$

Thus the mass of a reaction product can be determined[23], when the time-of-flight t over the distance d is measured in conjunction with the energy E. This can be achieved by detecting the particle with a silicon surface barrier detector, which provides a fast stop signal for the timing of the particle's flight over the distance d. The start signal may be obtained by bunching the projectile beam or by locating a transmission detector in the flight path at a distance d from the stop detector.

[23]R.R. Betts, Nucl. Inst. Meth. **162** (1979) 531.

Beam bunching[24] can produce beam pulses with widths of $\Delta t_{FWHM} \leq 150$ ns. This method has been used in this work for the identification of fission fragments. The time-of-flight of the evaporation residues from ^{40}Ca + ^{90,96}Zr was measured with the alternative technique using a transmission detector, which picked up the electrons produced when the residues penetrated through a thin carbon foil. Of the order of 100 low energy electrons are emitted from such foils after passage of a heavy ion. The detection of these electrons can be achieved, when they are accelerated near the foil by an electric field with a potential difference of the order of several keV and directed onto an electron detector, such as the microchannel plate multiplier[25]. A micro channel plate multiplier consists typically of a thin glass plate with closely spaced fine holes passing through it. These microchannels, which may have diameters as small as 20μm, have a secondary electron emitting surface which multiplies the number of electrons. An amplification of the order of 10^4 can be accomplished. The electrons are then collected by an anode. The total electron transit time through a microchannel is a few ns and the spread in timing is about 100 ps. In conjunction with a silicon surface barrier stop detector a time resolution of $\Delta t_{FWHM} \approx 150$ ps can be achieved.

2.3 Monitoring of the Projectile-Flux

The differential cross section of a nuclear reaction $d\sigma/d\Omega$, which in this work is often referred to simply as $d\sigma$, is for some scattering angle θ given by

$$\frac{d\sigma}{d\Omega}(\theta) = \frac{R(\theta)}{IN} \tag{2.11}$$

where $R(\theta)$ is the rate of events detected in the solid angle $d\Omega$, N is the number of target nuclei per unit area and I the current of incident nuclei per unit time. These three parameters are therefore the quantities to be measured in order to establish the differential cross section. Thus during the measurement of a particular reaction cross section apart from the actual reaction rate $R(\theta)$, the incident flux of nuclei I has to be monitored.

In this work the beam monitoring was performed to high precision with silicon surface barrier detectors located at forward angles, downstream from the target. At

[24]G.W. Butler *et al.*, Phys. Rev. Lett. **38** (1977) 1380.

[25]J.L. Wiza, Nucl. Inst. Meth. **162** (1979) 587.

these angles, even for bombarding energies well above the Coulomb barrier, the detected projectile nuclei have been elastically scattered. Since the elastic scattering is entirely due to the Coulomb interaction between projectile and target nucleus, it can be described with Rutherford's scattering formula (1.66). Thus with Equation 2.11 the incident flux I can be expressed as

$$I = \frac{R^R(\theta^M)}{N} \left[\frac{d\sigma^R(\theta^M)}{d\Omega} \right]^{-1} \tag{2.12}$$

where $R^R(\theta^M)$ is the rate of Rutherford scattering detected by a monitor detector at θ^M. It follows that

$$\frac{d\sigma}{d\Omega}(\theta) = \frac{R(\theta)}{R^R(\theta^M)} \frac{d\sigma^R}{d\Omega}(\theta^M) \tag{2.13}$$

Consequently, the density of target nuclei N cancels out and $R(\theta)$ and $R^R(\theta^M)$ become the only experimental quantities. In addition, the difference in solid angle between the monitor detector and the detector for the reaction products has to be accounted for. This can be accomplished by observing Rutherford scattering in both of these detectors.

In practice the beam direction is not always exactly along the axis with $\theta = 0°$ and it can be slightly different for different beam energies. The latter can be caused by the complex beam transport system, which cannot always be set in a consistent way. In order to correct for directional deviations of the beam, it may be monitored on both sides, e.g. at $\pm\theta^M$, in the plane in which the largest deviations occur. Taking the average rate of the two monitor detectors then automatically corrects for changes in the beam direction in this plane to first order. This method can be extended, when four monitor detectors are used, which are located at the same θ^M with the same distance from the target, but at the four corners of a square. The correct beam direction can then be obtained by comparing the rates for Rutherford scattering in these four detectors. In order to reduce the count rates to a manageable size and to accurately define the monitor detection angle θ^M, tantalum collimators with diameters of $\lesssim$ 1mm can be mounted in front of the monitor detectors.

2.4 Detection of Quasi-Elastic Scattering

The quasi-elastic scattering excitation functions which are discussed in Chapter 3 have been measured with two different methods. For the ^{16}O and ^{32}S reactions the scattered projectile-like nuclei have been detected at backward angles. For the ^{40}Ca reactions the recoiling target-like nuclei have been detected at forward angles.

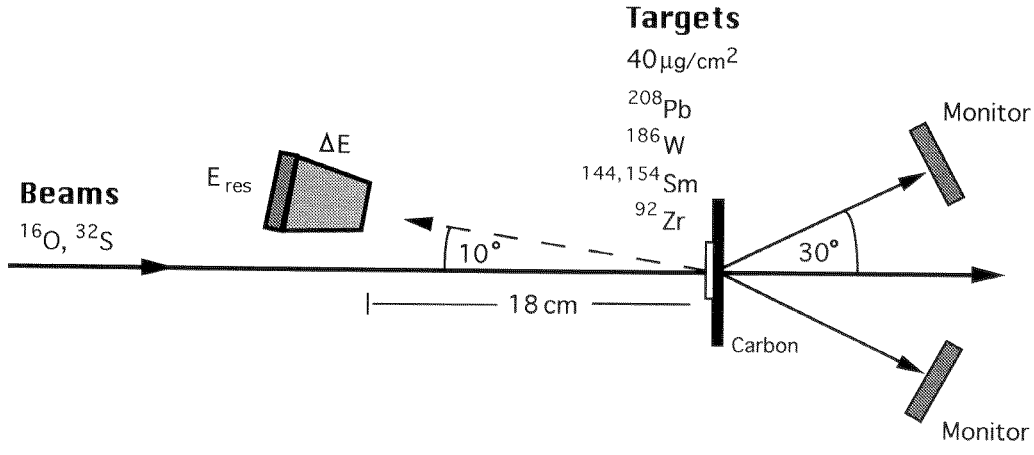

Figure 2.1: *The experimental set-up which was used in the detection of quasi-elastic scattering at backward angles.*

2.4.1 Detection at Backward Angles

The set-up used in the ^{16}O and ^{32}S experiments is illustrated in Figure 2.1. Two photographs of it are shown in Figure 2.4. A gas-ionization detector was positioned at an angle $\theta_{lab} = 170°$ relative to the beam direction. For some of the reactions quasi-elastic scattering was also measured at the angles $\theta_{lab} = 143°$ and 155°. The detector operated with 60 torr of propane and measured the energy loss ΔE of the scattered particles. It was backed by a silicon surface-barrier detector which measured their residual energy E_{res}. For each beam energy the combined information from these two detectors allowed the identification of the atomic number of the detected nuclei, as shown in Figure 2.2(a). For ^{16}O + ^{92}Zr, ^{144}Sm, the elastic events were clearly resolved from the inelastic events in the energy spectra, as it is shown in Figure 2.2(b). This allowed the elastic scattering differential cross sections to be extracted for these systems. For the other reactions the 'elastic' peak also contained some inelastic scattering from low-lying target states. The elastic scattering excitation functions established in this way are discussed in Chapter 4.

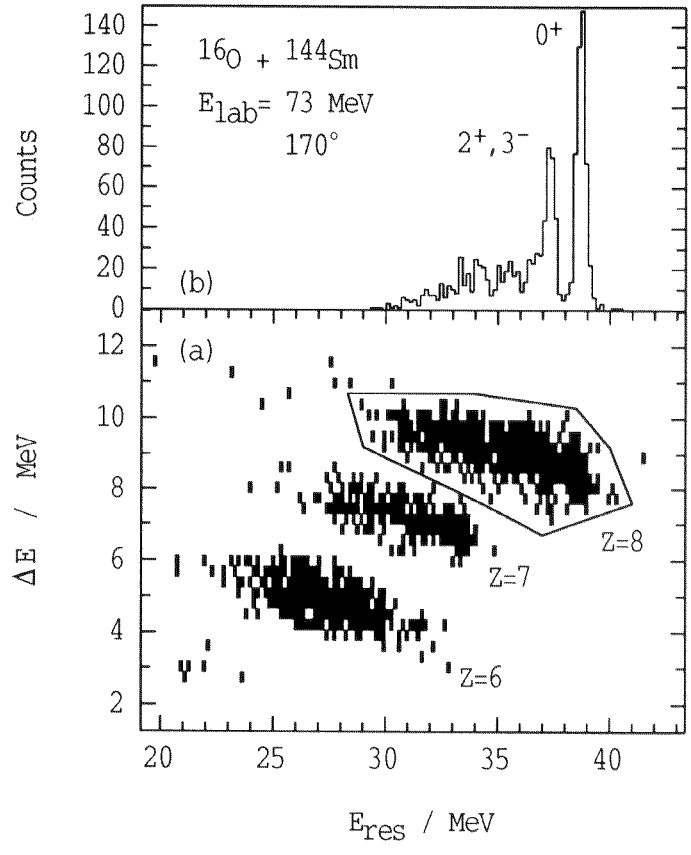

Figure 2.2: *Panel (a) shows the two-dimensional ΔE versus E_{res} spectrum for $^{16}O + ^{144}Sm$ at $E_{lab} = 73$ MeV and $\theta_{lab} = 170°$; the scattered particles are clearly separated according to their atomic numbers. Panel (b) shows the energy spectrum of the scattered oxygen nuclei; the channels associated with the 0^+ and the combination of the 2^+ and 3^- states of ^{144}Sm are resolved.*

2.4.2 Detection of Recoils at Forward Angles

The quasi-elastic scattering excitation functions for $^{40}Ca + ^{90,96}Zr$ have been measured through the detection of the recoiling zirconium-like nuclei in parallel with the fusion measurements for these systems. The recoils were detected in the four monitor detectors at $\theta_{lab} = 22°$. For elastic scattering the scattering angle of the recoiling target-like nucleus θ'_{lab} and the angle of the scattered projectile-like nucleus θ_{lab} are related in the laboratory system by

$$cos^2(\theta'_{lab}) = \frac{(A_p + A_t)^2}{4A_pA_t} - \frac{A_p}{4A_t}\left[cos(\theta_{lab}) + \sqrt{\frac{A_t^2}{A_p^2} - sin^2(\theta_{lab})}\right]^2 \qquad (2.14)$$

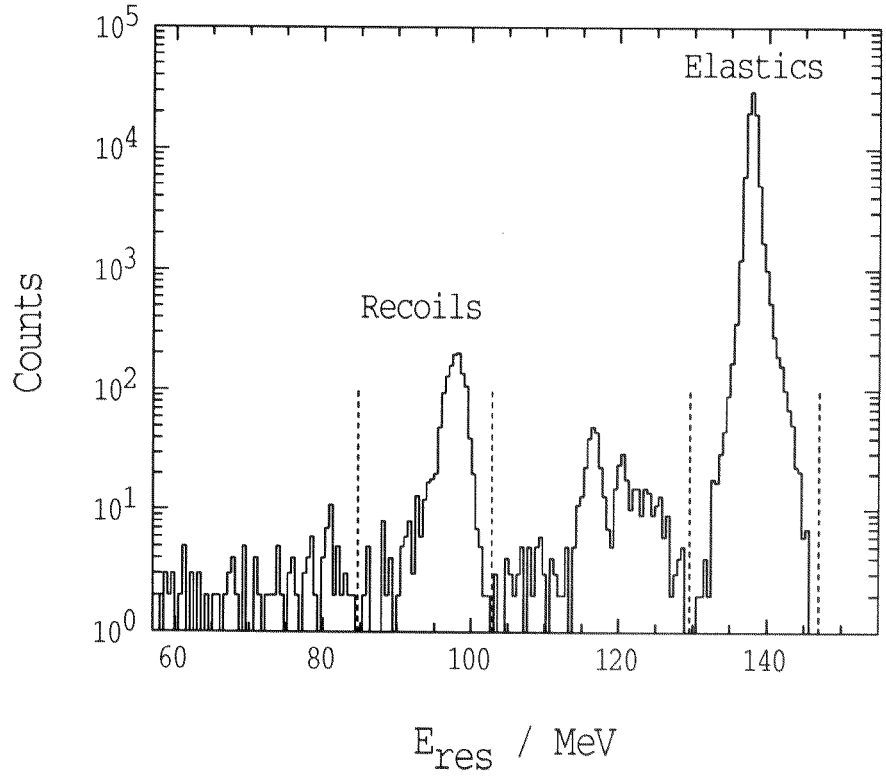

Figure 2.3: *A typical energy spectrum of the particles detected by one of the 22° monitor detectors. The overwhelming number of counts is comprised by the Rutherford scattering peak at 138 MeV. The recoil counts are contained in the peak at 98 MeV. The dashed lines indicate the positions of the gates.*

Thus for ^{40}Ca + ^{90,96}Zr the detection of a recoiling zirconium nucleus at $\theta'_{lab} = 22°$ corresponds to a scattered ^{40}Ca projectile at $\theta_{lab} = 111.6°$ for ^{90}Zr and $\theta_{lab} = 113.5°$ for ^{96}Zr, respectively. For both reactions the scattering angle of the calcium nucleus in the centre-of-mass system is $\theta_{c.m.} = 136°$, since

$$tan(\theta_{lab}) = \frac{sin(\theta_{cm})}{cos(\theta_{cm}) + A_p/A_t} \tag{2.15}$$

A typical energy spectrum of the particles detected with the 22° detectors is shown in Figure 2.3(b). In these spectra the recoil peak has been identified using its energy relation to the Rutherford scattering peak as given by the reaction kinematics. The recoil peaks have been integrated in the spectra of the four monitor detectors using a fixed gate which was shifted proportionally to the recoil energy. The number of counts have been reduced by a background estimate as obtained

from a region close to the peak. For each energy the recoil counts of the four detectors have been added and divided by the number of counts in the Rutherford scattering peak. The differential quasi-elastic scattering cross sections $d\sigma^{qel}$ have been normalized to the Rutherford differential cross section $d\sigma^{R}$, so that the data points at the lowest energies equal unity.

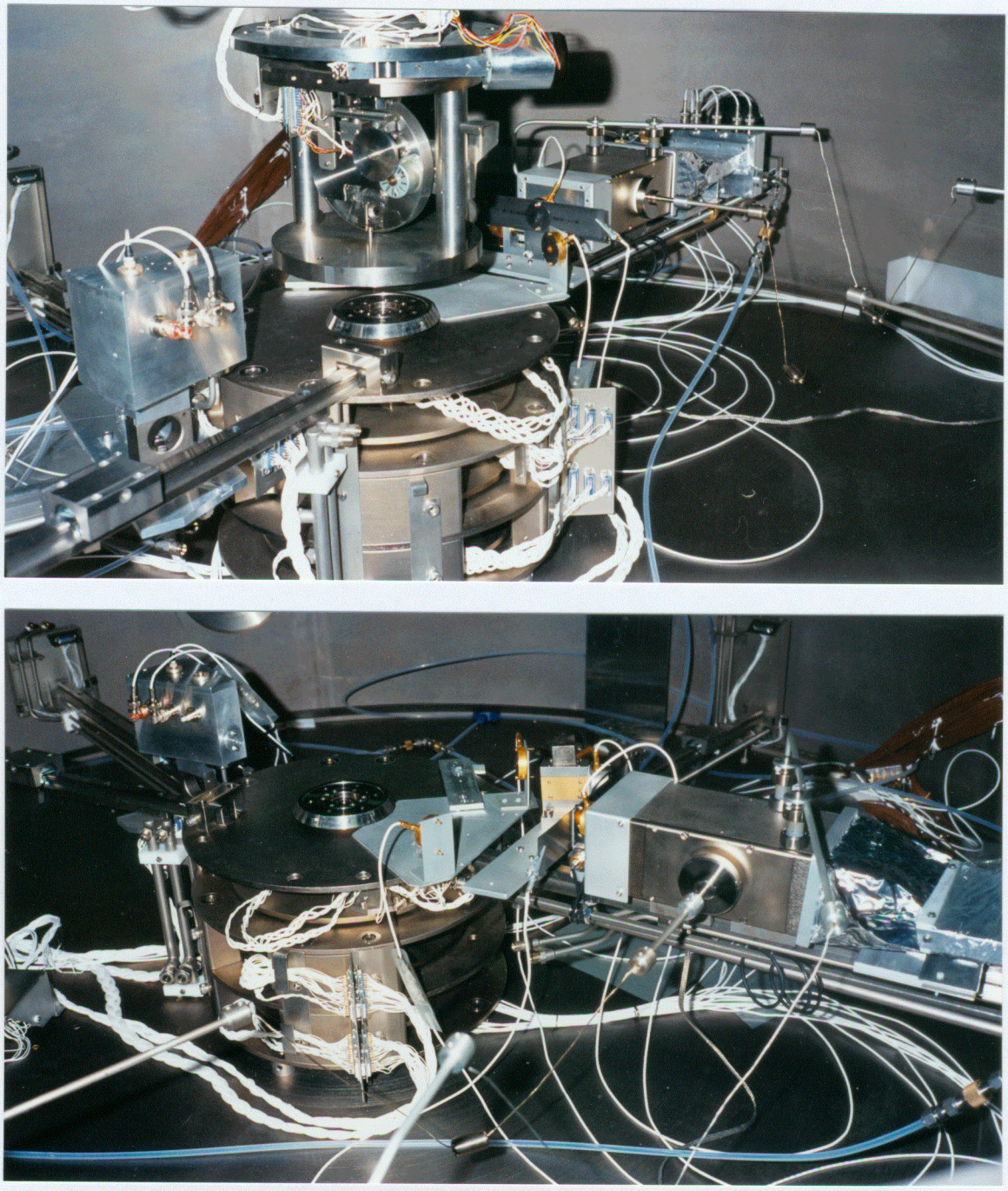

Figure 2.4: *The set-up in the 2 m scattering chamber of the Nuclear Physics Department at the ANU for the detection of evaporation residues and quasi-elastic scattering. For both photos the beam direction is from left to right. The upper photo shows the target wheel about 10 cm above its position during the experiments. The photos have been taken at* $\theta_{lab} \simeq 225°$ *(top) and* $\theta_{lab} \simeq 315°$ *(bottom). The scattering detector is at* $\theta_{lab} \simeq 170°$*, whereas the velocity filter and the evaporation residue detector are at* $\theta_{lab} \simeq 355°$*. Two silicon surface barrier detectors housed by brass cans are at* $\theta_{lab} \simeq 30°$ *and* $330°$*. They act as beam monitors.*

2.5 Detection of Evaporation Residues

As pointed out in Section 1.4 for binary systems with the combined charge number $Z_c \lesssim 70$ the decay of the fused system is dominated by particle evaporation. Thus the evaporation residue cross section can be identified with the fusion cross section. The fusion excitation functions for ^{40}Ca + ^{90,96}Zr, which are discussed in Chapter 5, have therefore been established through precision measurements of the residue cross sections. Similarly the fusion excitation functions for the systems ^{16}O + ^{92}Zr, ^{144,154}Sm, which are used in Chapters 3 and 4 for comparison with the scattering data, have been derived in other work[26,27] from evaporation residue measurements. For the systems ^{16}O + ^{186}W, ^{208}Pb evaporation residue and fission cross sections had to be combined to obtain the fusion excitation function.

The angular distribution of the evaporation residue differential cross sections is limited to small scattering angles and it is centered at 0°. Thus the detection of evaporation residues requires them to be separated from the intense flux of beam-like particles at these angles. For a typical total particle current of 10^9 particles per second of the order of 10^7 beam-like particles per second have to be rejected to obtain manageable count rates. This can be achieved using the transverse electrostatic field of an *electrostatic deflector* or using the combination of an electrostatic and a magnetostatic field, i.e. a *velocity filter*. After having been pre-selected in one of these ways the identification of residues and beam-like particles can then be accomplished by measuring their time-of-flight and energy.

2.5.1 Electrostatic Deflector

The fusion excitation functions for ^{40}Ca + ^{90,96}Zr were measured using the electrostatic deflector at the Legnaro Laboratories. This device[28] is illustrated in Figure 2.5.

The deflector features two adjustable pairs of electrodes which separate particles according to their electrical rigidity E/q, where E is the energy and q the charge state of the particle. For small deflection angles the trajectory of a charged particle inside a pair of electrodes follows to first order a section of a circle with radius r,

[26] J.R. Leigh *et al.*, Phys. Rev. C **52** (1995) 3151.

[27] J.C. Mein *et al.*, *to be published.*

[28] S. Beghini *et al.*, Nucl. Inst. Meth. A **239** (1985) 585.

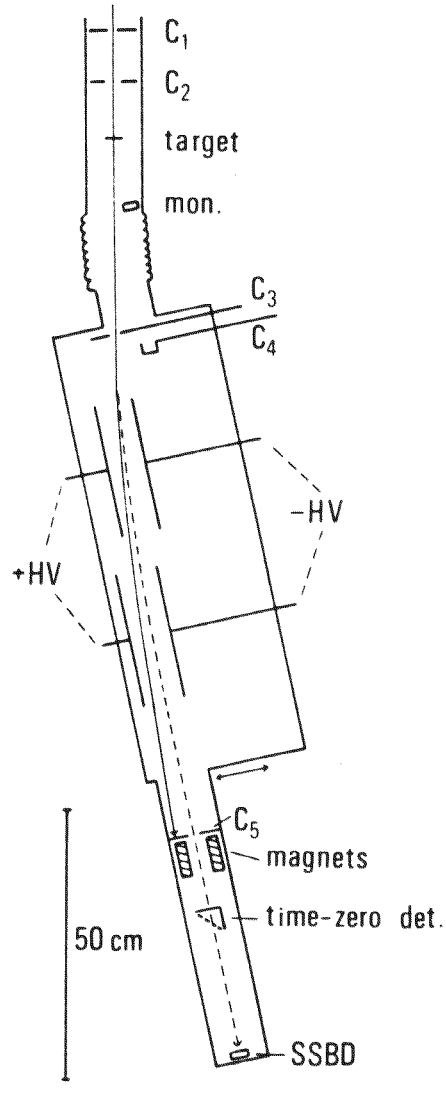

Figure 2.5: *The electrostatic deflector used to measure the fusion excitation functions for* $^{40}Ca + {}^{90,96}Zr$. *From top to bottom, the beam is focused onto the target through two collimators* (C_1, C_2) *which define the beam position and direction. The transmitted beam, the evaporation residues and other reaction products enter the deflector through an aperture* (C_3). *At this point the beam current can be monitored with a Faraday cup* (C_4). *Most of the beam-like particles are separated from the residues in the two transverse electric fields and stopped* (C_5). *The transmitted particles pass through a time-zero detector with micro-channel plates before their energy is measured by a silicon surface-barrier detector (SSBD). The combined timing information of the time-zero and the SSB detectors yields the time-of-flight of the particles over approximately 30 cm. Permanent magnets prevent electrons from entering the detection telescope.*

so that

$$\frac{mv^2}{r} \approx q\mathcal{E}, \tag{2.16}$$

where m is the particle's mass, v its velocity and $\mathcal{E}$ is the electric field. Consequently, the ratio of radii for beam-like particles (B) and evaporation residues (ER) is given by

$$\frac{r_{ER}}{r_B} \approx \frac{(E/q)_{ER}}{(E/q)_B} \approx \frac{(mq)_B}{(mq)_{ER}}. \tag{2.17}$$

The last step in this equation makes use of the fact that for small scattering angles because of momentum conservation the linear momenta of beam-like particles and residues are very similar. Since in a typical reaction the charge state of the residues is typically higher and their mass is usually more than twice than that of the beam-like particles, the trajectories of the former are bent more strongly than those of the latter. This results in a spatial separation of the two components.

The voltages applied to the plate electrodes are chosen, so that the evaporation residues are directed onto the aperture of a collimator at the end of the device. All other particles are stopped on this collimator. Typical deflection volts are of the order of 100 kV. The deflector reduces the number of beam-like particles sufficiently to be operated at the smallest scattering angles including 0°.

The geometric solid angle of the deflector is 0.636×10^{-4} sr as defined by the entrance aperture. Because of the existence of a distribution of charge states rather than a single charge state and because of varying velocities, the two electric fields have a defocusing effect. The evaporation residues are dispersed in the horizontal plane. Consequently the effective solid angle of the detection telescope following the deflector is smaller than the geometric one and the transmission of the device is less than unity.

Since the charge state distribution depends on the particular reaction measured, the transmission of the deflector was determined in this project for the system ^{40}Ca + ^{96}Zr at scattering angles $\theta_{lab} = 4°$ and 6° for $E_{lab} = 152$ MeV, by comparing the yields of evaporation residues with and without deflection. It was found that the defocusing effect of the electric fields reduces the transmission in this case from unity to 0.7 ± 0.05. This result has been adopted for the two systems measured in this work for all energies and angles.

2.5.2 Velocity Filter

The dispersion associated with electrostatic deflectors can be reduced, if the plate electrodes are located inside a magnetic field, with the magnetic field direction perpendicular to the electric field, so that the electric and magnetic forces counteract each other[29]. If the deflection is small the force acting on a charged particle in such a device is given to first order by

$$F \approx qv\mathcal{B} - \mathcal{E} \tag{2.18}$$

Thus for a given velocity the electric and the magnetic field can be adjusted, so that independent of the charge state the net force is zero. In fact, the device acts as a velocity filter by forcing all particles with the chosen velocity independent of their charge state on a straight trajectory. Particles with other velocities are deflected away from this trajectory and can be stopped. The charge independence of the method excludes dispersion of the residues due to the existence of different charge states. A small dispersion effect, however, persists because of the velocity differences between the residues. Optimum separation between residues and beam-like particles can be achieved, when the two components are deflected in opposite directions. Such a velocity filter[30] has been used for the precision measurements of the evaporation residue cross sections for the systems ^{16}O + ^{92}Zr, ^{144,154}Sm, ^{186}W and ^{208}Pb at the ANU, which have been documented elsewhere[31]. The experimental set-up for these fusion measurements is illustrated in Figure 2.6. It is shown in two photographs in Figure 2.4.

2.5.3 Identification of Evaporation Residues

In both the ANU and the Legnaro set-up the time-of-flight and the residual energy E_{res} are measured for the evaporation residues and the remaining beam-like particles which are not rejected by the velocity filter or the electrostatic deflector. This enables a complete separation of the residues from background. At the ANU the projectile beam is bunched and the beam bunching is used as a time reference which serves as stop signal. A fast signal from the E_{res} detector which is downstream from the velocity filter is used to start the timing. Beam pulsing is not necessary

[29]W. Wien, Ann. Physik **65** (1898) 440; **8** (1902) 260.

[30]J.X. Wei *et al.*, Nucl. Inst. Meth. **A 306** (1991) 557.

[31]J.R. Leigh *et al.*, Phys. Rev. C **52** (1995) 3151.

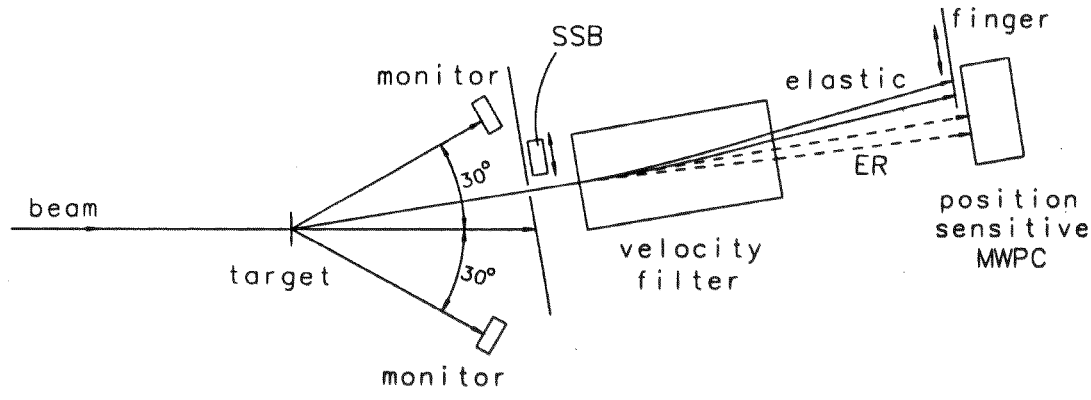

Figure 2.6: *From left to right, the beam is directed onto the target and is monitored by two silicon surface barrier detectors at 30° which detect Rutherford scattering. The reaction products proceed through a collimator into the velocity filter, where most of the intense flux of beam-like particles is intercepted by a tantalum finger. The remaining particles are detected by a position sensitive multi-wire proportional counter (MWPC). A silicon surface barrier detector (SSB) behind the collimator can be used to measure the solid angle of the aperture. The velocity filter can be operated at angles as close as 0.5° to the beam direction. The measured transmission of the filter is very close to unity.*

for the set-up in Legnaro, where the residues and the remaining beam-like particles are detected by a microchannel plate detector after they leave the deflector. The artificially delayed signal of this transmission detector stops the timing. The timing is started by the fast signal of a silicon surface barrier detector 40 cm further downstream. This detector also measures the residual energy E_{res} of the particles. For both set-ups the combined TOF and E_{res} information enables a clean separation of the evaporation residues from other particles. This is demonstrated in Figure 2.7 which shows a typical two-dimensional TOF versus E_{res} spectrum for the reaction ^{40}Ca + ^{90}Zr measured in Legnaro.

2.6 Detection of Fission Fragments

The fission fragments originating from the reaction ^{32}S + ^{208}Pb were detected with two multi-wire proportional gas counters of the new fission fragment spectrometer at

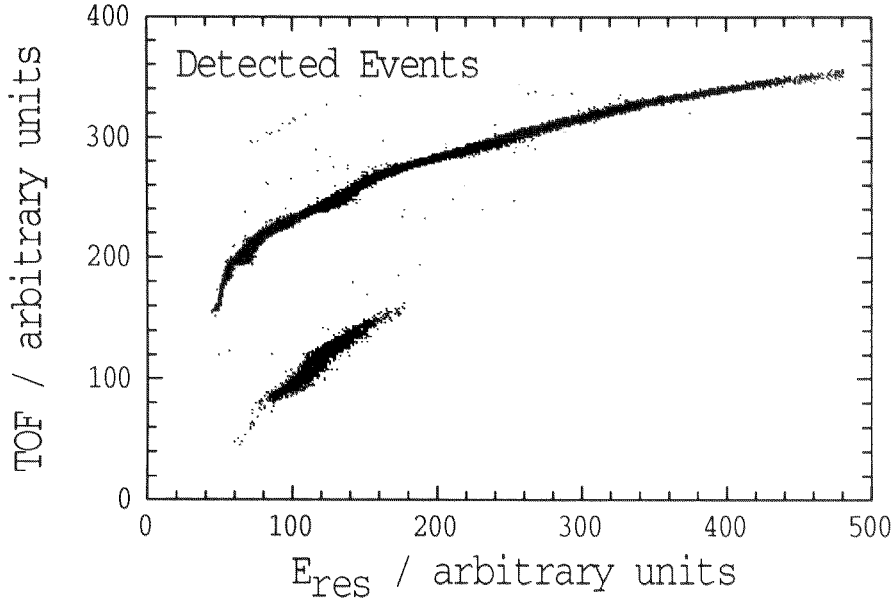

Figure 2.7: *The detected events for ^{40}Ca + ^{90}Zr at E_{lab} = 152 MeV plotted as a function of TOF and E_{res}. The evaporation residues in the lower part of the plot are cleanly separated from the beam-like particles above.*

the ANU, see also Reference[32]. The multi-wire proportional counters were located, so that they detected fragments at forward and backward angles, respectively. The counters were inside a vacuum chamber that operated at pressures of 2×10^{-6} Torr.

Each of these counters consists of a plane of vertical and a plane of horizontal wires located 3 mm either side of a central cathode foil. The wires of each plane are connected by delay-chips. The timing of signals from these delay-lines thus enables the coordinates of the ionizing event in x- and y-direction to be obtained. The cathode-foil is made of gold-coated polyethylene. To reduce the capacitance of the foil it is segmented into four sectors. The operating voltages applied to the counters are typically 500 V. They use propane at a gas pressure of approximately 4 Torr, which is maintained by a gas-flow system. The counters are separated from the vacuum by a copper-coated polyethylene foil.

Each counter gives the x- and y-position of the event, the energy loss ΔE of the fragment and its TOF relative to the bunched beam. The fission fragments

[32]C.R. Morton, *Ph.D.-thesis*, Australian National University (1995).

have been identified using the ΔE and TOF signals. The position information was calibrated using elastic scattering from a 200 μg/cm^2 ^{197}Au target. The beam was monitored through the detection of Rutherford scattering in two silicon surface barrier detectors at forward angles.